Cancer Research

Validation and Structural Characterization of the LEDGF/p75–MLL Interface as a New Target for the Treatment of MLL-Dependent Leukemia

Kateřina Čermáková[1], Petr Tesina[2,3], Jonas Demeulemeester[1], Sara El Ashkar[1], Hélène Méreau[4], Juerg Schwaller[4], Pavlína Řezáčová[2,5], Vaclav Veverka[2], and Jan De Rijck[1]

Abstract

Mixed lineage leukemia (MLL) fusion–driven acute leukemias represent a genetically distinct subset of leukemias with poor prognosis. MLL forms a ternary complex with the lens epithelium–derived growth factor (LEDGF/p75) and MENIN. LEDGF/p75, a chromatin reader recognizing H3K36me3 marks, contributes to the association of the MLL multiprotein complex to chromatin. Formation of this complex is critical for the development of MLL leukemia. Available X-ray data represent only a partial structure of the LEDGF/p75–MLL–MENIN complex. Using nuclear magnetic resonance spectroscopy, we identified an additional LEDGF/p75–MLL interface, which overlaps with the binding site of known LEDGF/p75 interactors—HIV-1 integrase, PogZ, and JPO2. Binding of these proteins or MLL to LEDGF/p75 is mutually exclusive. The resolved structure, as well as mutational analysis, shows that the interaction is primarily sustained via two aromatic residues of MLL (F148 and F151). Colony-forming assays in MLL–AF9^{+} leukemic cells expressing MLL interaction-defective LEDGF/p75 mutants revealed that this interaction is essential for transformation. Finally, we show that the clonogenic growth of primary murine MLL-AF9–expressing leukemic blasts is selectively impaired upon overexpression of a LEDGF/p75-binding cyclic peptide CP65, originally developed to inhibit the LEDGF/p75–HIV-1 integrase interaction. The newly defined protein–protein interface therefore represents a new target for the development of therapeutics against LEDGF/p75–dependent MLL fusion–driven leukemic disorders. *Cancer Res; 74(18); 5139–51. ©2014 AACR.*

Introduction

The mixed lineage leukemia (*MLL*) gene, located on chromosome 11q23, is frequently targeted by chromosomal translocations (see Krivtsov and Armstrong for a review; ref. 1). Balanced rearrangements result in the formation of new fusion proteins involved in childhood and adult *de novo* as well as therapy-related myeloid and lymphoblastic leukemias. Wild-type (WT) MLL is a histone methyltransferase associated with the promoters of a large subset of active genes. More specifically, MLL maintains the expression of posterior *HOXA* genes (*HOXA5*, *HOXA9*, and *HOXA10*) and as such is essential for embryonic body plan formation and the self-renewal capacity of hematopoietic stem cells and immature progenitors (2, 3).

Typical MLL oncogenic fusions retain the MLL N-terminal region. To date, more than 70 different N-terminal fusions associated with leukemia development have been identified, of which MLL–AF4, MLL–AF9, and MLL–ENL originate from t(4;11), t(9;11), and t(11;19) translocations, respectively, and are the most prevalent (Fig. 1A; ref. 4). These fusion partners are part of a complex converting promoter-proximal arrested RNA Pol II into the elongation state (5), which suggests that a subset of MLL-mediated leukemias is triggered by aberrant transcriptional elongation. The mechanism whereby other MLL fusion partners initiate cellular transformation is, however, largely unknown. Recent studies also suggest that reciprocal MLL fusion proteins may have an important role in cancer development (6, 7) and that MLL fusions also need the functional activity of the WT MLL protein to maintain oncogenic transformation (8).

Although MLL can bind directly to DNA via its AT-hooks and CXXC-domain, the MLL multiprotein complex is targeted to specific genes through interaction with various cellular proteins inducing gene activation or repression (9). Among others, MLL forms a ternary complex with MENIN (MEN1) and the

[1]KU Leuven, Laboratory for Molecular Virology and Gene Therapy, Department of Pharmaceutical and Pharmacological Sciences, Leuven, Belgium. [2]Institute of Organic Chemistry and Biochemistry of the ASCR, v.v.i., Structural Biology, Prague, Czech Republic. [3]Charles University in Prague, Department of Genetics and Microbiology, Faculty of Science, Prague, Czech Republic. [4]Department of Biomedicine, University Hospital and Children's Hospital Basel (UKBB) ZLF, Basel, Switzerland. [5]Institute of Molecular Genetics of the ASCR, v.v.i., Structural Biology, Prague, Czech Republic.

Note: Supplementary data for this article are available at Cancer Research Online (http://cancerres.aacrjournals.org/).

V. Veverka and J. De Rijck shared senior authorship for this article.

Corresponding Authors: Jan De Rijck, KU Leuven, Molecular Virology and Gene Therapy, Kapucijnenvoer 33, VCTB +5, 3000 Leuven, Belgium. Phone: 32-16-33-21-76; Fax: 32-16-33-63-36; E-mail. Jan.Derijck@med.kuleuven.be; and Vaclav Veverka, IOCB ASCR, Flemingovo nam. 2, 16610 Prague, Czech Republic; Phone: 420-220-183-135; E-mail: veverka@uochb.cas.cz

doi: 10.1158/0008-5472.CAN-13-3602

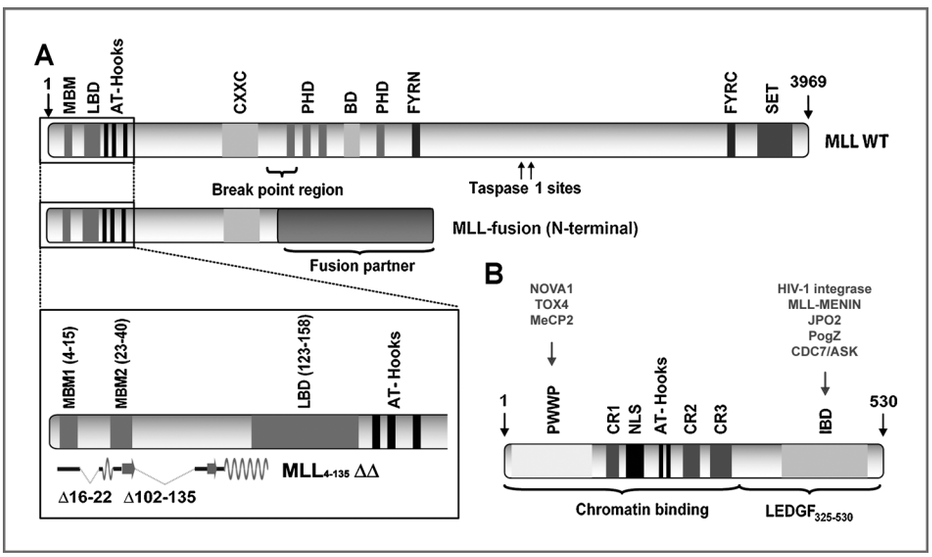

Figure 1. Schematic representation of the domain structure of MLL, MLL fusions, and LEDGF/75. A, schematic representation of the domain structure of WT MLL and N-terminal MLL fusion proteins. MLL contains several domains involved in chromatin binding—AT-Hooks, a cysteine rich domain (CxxC), four plant homeodomains (PHD) fingers, and a bromodomain (BD). The MLL protein is expressed as a single polypeptide chain cleaved by taspase 1 into two fragments, which associate by noncovalent interactions between the FY-rich domain N-terminal (FYRN) and FY-rich domain C-terminal (FYRC). The suppressor of variegation enhancer of zeste and trithorax (SET) domain at the C-terminal end is responsible for the methyltranferase function. The breakpoint region indicates the location where fusion partners are merged with part of the MLL protein. The N-terminal end of MLL contains two MBM1 and 2 (MBM) and the LBD. The structure of the $MLL_{4-135}\Delta\Delta$ peptide was determined in the published LEDGF/p75–MLL–MENIN ternary complex (PDB ID 3U88). The secondary structure of resolved areas of MLL is indicated schematically. B, schematic representation of the domain structure of LEDGF/p75. At the N-terminal end, a Pro-Trp-Trp-Pro (PWWP) domain is situated, recognizing H3K36me3 marks followed by the first charged region (CR1), the nuclear localization signal (NLS), two AT-Hooks, and two additional charged regions (CR2 and CR3). These domains are involved in chromatin recognition. The IBD, important for the interaction of LEDGF/p75 with the MLL–MENIN complex is situated at the C-terminal part of the protein. The currently known binding partners of LEDGF/p75 are listed above the LEDGF/p75 cartoon. Methyl-CpG-binding protein 2 (MeCP2), neuro-oncological ventral antigen 1 (NOVA1), and TOX high mobility group box family member 4 (TOX4) interact with the PWWP domain and HIV-1 integrase, the MLL–MENIN complex, JPO2, Pogo transposable element with ZNF domain (PogZ), and Cdc7-activator of S-phase kinase (CDC7/ASK) interact with the IBD.

lens epithelium–derived growth factor (LEDGF/p75) via the N-terminal MENIN binding motifs (MBM1, 2) and the LEDGF/p75 binding domain (LBD), respectively (Fig. 1A; refs. 10–12). Both MENIN and LEDGF/p75 are essential for MLL fusion–mediated transformation (11, 12). LEDGF/p75 is an epigenetic reader recognizing H3K36me3 marks via its PWWP domain and as such it preferentially associates with the body of actively transcribed genes (Fig. 1B; refs. 13–15). Alongside the MLL complex, LEDGF/p75 is known to target several other proteins or protein complexes to chromatin including JPO2, the pogo transposable element with ZNF domain (PogZ), and human immunodeficiency virus type 1 (HIV-1) integrase (16–19). In this regard, LEDGF/p75 was shown to determine the HIV integration site preference and was shown to be important for HIV-1 replication (20–22). Most LEDGF/p75-interacting proteins, including the MLL complex, interact with the LEDGF/p75 integrase binding domain (IBD; Fig. 1B). MENIN functions as a scaffold protein stabilizing the interaction between MLL and LEDGF/p75. It was shown that replacement of the MLL–MENIN binding domain by the PWWP domain is sufficient to rescue leukemic transformation in the absence of MENIN (12).

We have previously shown that stable overexpression of the C-terminal fragment of LEDGF/p75 (aa 325–530, $LEDGF_{325-530}$; Fig. 1B) containing the IBD, but lacking the PWWP domain, outcompetes endogenous LEDGF/p75 from the MLL–MENIN complex and dramatically reduces clonogenic growth of hematopoietic stem cells immortalized by MLL fusion proteins both *in vitro* and in a mouse model (23). Similar results were obtained with small molecules targeting the MLL–MENIN interaction (24). The existence of a ternary complex comprising LEDGF/p75, MLL, and MENIN is supported by the available crystal structure (Supplementary Fig. S1A; ref. 25). This structure represents the assembly of close to full-length MENIN, the IBD of LEDGF/p75, and an MLL-derived peptide comprising amino acids (aa) 4 to 135, which was further engineered by removal of unstructured regions (aa 16–22 and 36–102; $MLL_{4-135}\Delta\Delta$); Fig. 1A; Supplementary Fig. S1A). Huang and colleagues used isothermal titration calorimetry (ITC) to show that the LEDGF/p75 IBD binds the MLL–MENIN complex with high affinity, whereas neither MENIN nor $MLL_{4-135}\Delta\Delta$ alone stably associate with LEDGF/p75. In contrast, we were able to detect an interaction between LEDGF/p75 and an N-terminal MLL-derived fragment (aa 1–160) in the absence of MENIN using AlphaScreen technology (23). Moreover, we previously showed that a LEDGF/p75 IBD-derived peptide spanning aa 375 to 386 ($LEDGF_{375-386}$) inhibited the LEDGF/p75–MLL_{1-160} interaction and leukemic transformation (Supplementary Fig. S1B; ref. 23). Because none of these LEDGF/p75 residues are in direct contact with MLL in the published structure, these data hint toward the existence of an additional important interaction between MLL and LEDGF/p75.

In this article, we identify and structurally characterize a novel LEDGF/p75–MLL interface. We show that the LEDGF/p75 IBD interacts with MLL via the same binding site as other known LEDGF/p75 binding proteins including HIV-1 integrase, PogZ, and JPO2 (16, 17, 26). In addition, we show that LEDGF/p75 interacting peptides known to inhibit the LEDGF/p75–HIV-1 integrase interaction impair clonogenic growth of primary murine MLL fusion–expressing leukemic cells, which validates this interface as a new therapeutic target (27).

Materials and Methods

Generation of retroviral vectors

Murine stem cell virus–based (*pMSCV*) retroviral vector production was performed as described previously (28). Production of Simian immunodeficiency virus (SIV)–derived vectors was performed as described earlier (29). Briefly, vesicular stomatitis virus glycoprotein pseudotyped SIV-based particles were produced by poly(ethylenimine) transfection in 293T cells using the indicated transfer plasmids, the pAd-SIV3$^+$ packaging plasmid (a kind gift from Didier Nègre, Ecole Normale Supérieure, Lyon, France) and the envelope expression plasmid pMD.G.

Culture and generation of THP1 cells expressing LEDGF/p75

THP1 human MLL–AF9$^+$ acute myeloid leukemia (AML) cells were maintained in Roswell Park Memorial Institutes medium (RPMI-1640; Gibco-BRL) supplemented with 10% heat-inactivated fetal bovine serum (FBS; Gibco, Invitrogen) and 50 μg/mL gentamycin (Gibco, Invitrogen). To create cells stably expressing LEDGF/p75 or LEDGF/p75 L368A-K407D, cells were transduced with the respective SIV vectors or an empty control vector and selected with 0.5 mg/mL of hygromycin B (Clontech).

Generation and transduction of murine MLL–AF9-expressing AML cells

Murine MLL–AF9-expressing AML cells were generated by transplantation of bone marrow cells stably transduced to express MLL–AF9 using a previously published protocol with some modifications (30). In brief, bone marrow cells were harvested from 8-week-old (FVB/Nx129/S1) F1 mice and enriched for progenitors using a lineage-marker-depletion progenitors kit (Cell Mag Kit; R&D Systems). These cells were cultured for 24 hours in RPMI-1640 [10% FCS, 1% penicillin/streptomycin, 10 ng/mL of human interleukin-6 (IL6), 6 ng/mL of murine IL3, and 100 ng/mL of murine stem cell factor] before transduction with a MSCV-derived retroviral vector encoding MLL–AF9 by spinoculation (2,000 × *g*, 90 minutes at 306 K) on two consecutive days. After the second spinoculation, 5×10^5 transduced bone marrow cells were injected into the tail vein of lethally irradiated (950 rad) syngeneic recipients. As described previously and as shown in Supplementary Fig. S2, 100% of the mice developed AML after a median latency of 75 days. Leukemic cells were harvested from the bone marrow of diseased mice and expanded in medium containing growth factors until the next round of transduction using the protocol described above with *pMSCV eGFP-PGK-puro*, *pMSCV CP65 eGFP-PGK-puro*, or its mutant variants. Cells were flow-sorted for eGFP expression 24 hours after transduction before analysis.

Clonogenic growth assays *in vitro*

MLL–AF9$^+$-expressing murine leukemic cells (described above) or normal bone marrow progenitors cells were plated in methylcellulose containing 6 ng/mL IL3, 10 ng/mL IL6, and 100 ng/mL murine stem cell factor (M3534; STEMCELL Technologies) in the presence of 2 μg/mL puromycin. Five to 7 days later, the number of colonies was determined.

For the clonogenic growth assay with THP1-derived cells, cells were seeded in a 96-well plate (1×10^5 cells/well) and transduced with a lentiviral vector expressing GFP and a miRNA targeting LEDGF/p75 or a GFP control vector. After 24 hours, cells were selected with puromycin (4 μg/mL). Forty-eight hours after transduction, 5×10^3 cells were plated in methylcellulose medium (M3534; STEMCELL Technologies) in the presence of hygromycin (0.5 mg/mL) and puromycin (4 μg/mL). Remaining cells were expanded in culture for 2 days for Western blot analysis. The number of colonies was determined after 10 days.

Reverse transcription quantitative PCR

qRT-PCR analysis of the HoxA9 mRNA expression level was performed as described previously (23). The sequences of all used primer pairs are indicated in Supplementary Table S1.

NMR spectroscopy and structural calculations

All nuclear magnetic resonance (NMR) data were acquired at 298 K on a 600 MHz Bruker Avance spectrometer equipped with triple-resonance (^{15}N/^{13}C/^{1}H) cryoprobe. NMR spectra were collected from 0.35 mL samples of 0.1 mmol/L ^{15}N-labeled LEDGF/p75 IBD for binding site mapping or 0.5 mmol/L equimolar solution of ^{13}C/^{15}N-labeled LEDGF/p75 IBD-unlabeled $MLL_{140–160}$ for resonance assignments and structural determination of the complex in a 25 mmol/L HEPES buffer, pH 7.0, containing 100 mmol/L NaCl, 0.05% 2-mercaptoethanol, 5% D_2O/95% H_2O. A series of double- and triple-resonance spectra were recorded to obtain essentially complete backbone and side-chain resonance assignments for the $MLL_{140–160}$-bound ^{13}C/^{15}N-labeled LEDGF/p75 IBD (31, 32). The assignments for the bound $MLL_{140–160}$ peptide were obtained using ^{13}C/^{15}N-filtered homonuclear TOCSY and NOESY experiments. ^{1}H-^{1}H distance constraints required to calculate the structure of the LEDGF/p75 IBD–$MLL_{140–160}$ complex were derived from 3D ^{15}N/^{1}H NOESY-HSQC, ^{13}C/^{1}H HSQC-NOESY, and in 2D ^{13}C/^{15}N-filtered/edited NOESY spectra, which were acquired with an NOE mixing time of 120 milliseconds. Specific interaction of the MLL-derived peptides with the LEDGF/p75 IBD was monitored by changes induced in the positions of signals of ^{13}C/^{15}N-labeled LEDGF/p75 IBD in 3D HNCO spectra (33, 34).

The family of converged structures for the LEDGF/p75 IBD–$MLL_{140–160}$ complex was initially calculated using Cyana 2.1, as described previously (33). The combined automated NOE assignment and structure determination protocol (35) was

used to automatically assign the NOE cross-peaks identified in 2D NOESY spectra, and to produce preliminary structures. In addition, backbone torsion angle constraints, generated from assigned chemical shifts using the program TALOS+ (36), were included in the calculations. Subsequently, five cycles of simulated annealing combined with redundant dihedral angle constraints were used to produce the sets of converged structures with no significant restraint violations (distance and van der Waals violations < 0.2 Å), which were further refined in explicit solvent in YASARA (http://www.yasara.org/). Analysis and validation of the family of structures obtained were carried out using the programs Molmol, iCING, and PyMol (37)

AlphaScreen

AlphaScreen measurements were performed in a final volume of 25 μL in 384-well Optiwell microtiter plates (PerkinElmer). All components were diluted in assay buffer [25 mmol/L Tris pH 7.4, 150 mmol/L NaCl, 1 mmol/L dithiothreitol , 0.1% (v/v) Tween-20, 1 mmol/L $MgCl_2$, and 0.1% (w/v) bovine serum albumin (BSA)]. The optimal binding concentration for each protein was determined in cross-titration experiments. For avidity determinations, $MLL_{1–160}$–GST WT (first 160 aa of MLL N-terminally fused to glutathione-*S*-transferase) and/or its mutants were titrated against 0.3 nmol/L Flag-tagged LEDGF/p75 (Flag-LEDGF/p75). Flag-LEDGF/p75 and/or its mutants were titrated against 10 nmol/L $MLL_{111–160}$–GST. For 50% inhibitory concentration (IC_{50}) determinations, MBP-JPO2, MBP-PogZ, HIV-1 integrase, CP65-MBP constructs, or maltose binding protein (MBP) were titrated against 1 nmol/L $MLL_{1–160}$–GST and 0.3 nmol/L Flag-LEDGF/p75. In outcompetition experiments, Flag-LEDGF/p75 was preincubated with MBP-JPO2, MBP-PogZ, HIV-1 integrase, CP65-MBP constructs, or MBP for 1 hour at 277 K. Subsequently, $MLL_{1–160}$–GST was added at the indicated concentrations. When all proteins were added, the plate was incubated for 1 hour at 277 K. Glutathione donor (20 μg/mL) and anti-Flag acceptor beads (PerkinElmer) were added, bringing all proteins to the indicated final concentrations. After 1 hour of incubation at 293 K, the plate was analyzed in an EnVision Multi-label Reader in AlphaScreen mode (PerkinElmer). Results were analyzed in Prism 5.0 (GraphPad software) after nonlinear regression with the appropriate equations: one-site specific binding, taking ligand depletion into account for the apparent K_d measurements and sigmoidal dose-response with variable slope for the IC_{50} determination.

Peptide synthesis

Peptides were synthesized by solid-phase synthesis in the Laboratory of Medicinal chemistry, IOCB, ASCR v. v. i. (Prague, Czech Republic).

Statistical analysis

Mean values and SDs were calculated to estimate the degree of variation as specified for each experiment. GraphPad Prism 5.0 software (Pnsm Software Corp.) was used for statistical analysis, unless stated differently.

Additional methods can be found in the Supplementary Data.

Results

Characterization of the LEDGF/p75–MLL interface

We first examined whether the described LEDGF/p75–MLL–MENIN interface is sufficient to support the LEDGF/p75–MLL interaction in the absence of MENIN. Through coimmunoprecipitation and assessment of the myeloid transformation capacity of MLL fusion proteins, Yokoyama and Cleary (12) suggested that MLL residue F129 (Supplementary Fig. S1C) is crucial to support MENIN-mediated binding of LEDGF/p75 to MLL. We therefore introduced this mutation into a recombinant protein comprising the first $MLL_{1–160}$–GST, which contains both the LEDGF/p75 and the MBM1 and 2 and compared its interaction with LEDGF/p75 to that of the WT variant. Integrity of all used recombinant proteins was confirmed by SDS-PAGE (Supplementary Fig. S3). WT $MLL_{1–160}$–GST readily interacted with recombinant triple Flag-LEDGF/p75 in an *in vitro* AlphaScreen assay (Fig. 2A). Interestingly, this interaction was only marginally affected by the F129A mutation. The published crystal structure of the ternary complex indicates that next to F129, F133 also contributes to the interaction with LEDGF/p75 (Supplementary Fig. S1C). Although the F129A, F133A double-mutant decreased the AlphaScreen signal, it failed to completely abolish the interaction with LEDGF/p75 (Fig. 2A). However, mutational analysis of conserved MLL residues outside the MLL fragment resolved in the crystal structure revealed that a triple-mutation (E144Q-E146Q-F148A) abolished the interaction with LEDGF/p75 (Fig. 2A). This observation indicates the existence of an additional LEDGF/p75–MLL interface.

We used NMR spectroscopy for a detailed characterization of the LEDGF/p75–MLL interface. In particular, we followed the changes in positions of backbone NMR signals of either ^{15}N or $^{13}C/^{15}N$-labeled LEDGF/p75 IBD (aa 345–426) in the presence of different synthetic MLL-derived peptides. The first peptide consisted of MLL aa 111 to 139 ($MLL_{111–139}$) and thus included the α helical region resolved in the published ternary structure. The second peptide comprised MLL aa 140 to 160 ($MLL_{140–160}$) not included in the resolved interface of the ternary complex. A third peptide (aa 123 to 160; $MLL_{123–160}$) combines residues from $MLL_{140–160}$ with the amino acid residues known to contribute to interaction with LEDGF/p75 (MLL F129 and F133). We compared the 2D $^{15}N/^{1}H$ HSQC spectrum of the ^{15}N-labeled IBD in the absence or presence of the unlabeled MLL-derived peptides. $MLL_{111–139}$ did not induce significant shifts in positions of the IBD backbone amide signals (Supplementary Fig. S4A). This observation is in agreement with the results of Huang and colleagues (25), who were unable to detect a binary interaction between the IBD and $MLL_{4–135}\Delta\Delta$ in the absence of MENIN. In contrast, both $MLL_{140–160}$ and $MLL_{123–160}$ induced significant chemical shift perturbations of the IBD backbone signals (Fig. 2B and Supplementary Fig. S3B, respectively). The specific shifts of IBD amino acid residues induced by addition of $MLL_{140–160}$ or $MLL_{123–160}$ were determined by comparison of the positions of the IBD backbone signals (HN, N, C') in 3D HNCO spectra (Fig. 2C and Supplementary Fig. S4C, respectively). Overall, the chemical shift perturbations in the IBD backbone induced by binding of $MLL_{140–160}$ and $MLL_{123–160}$ were found in two

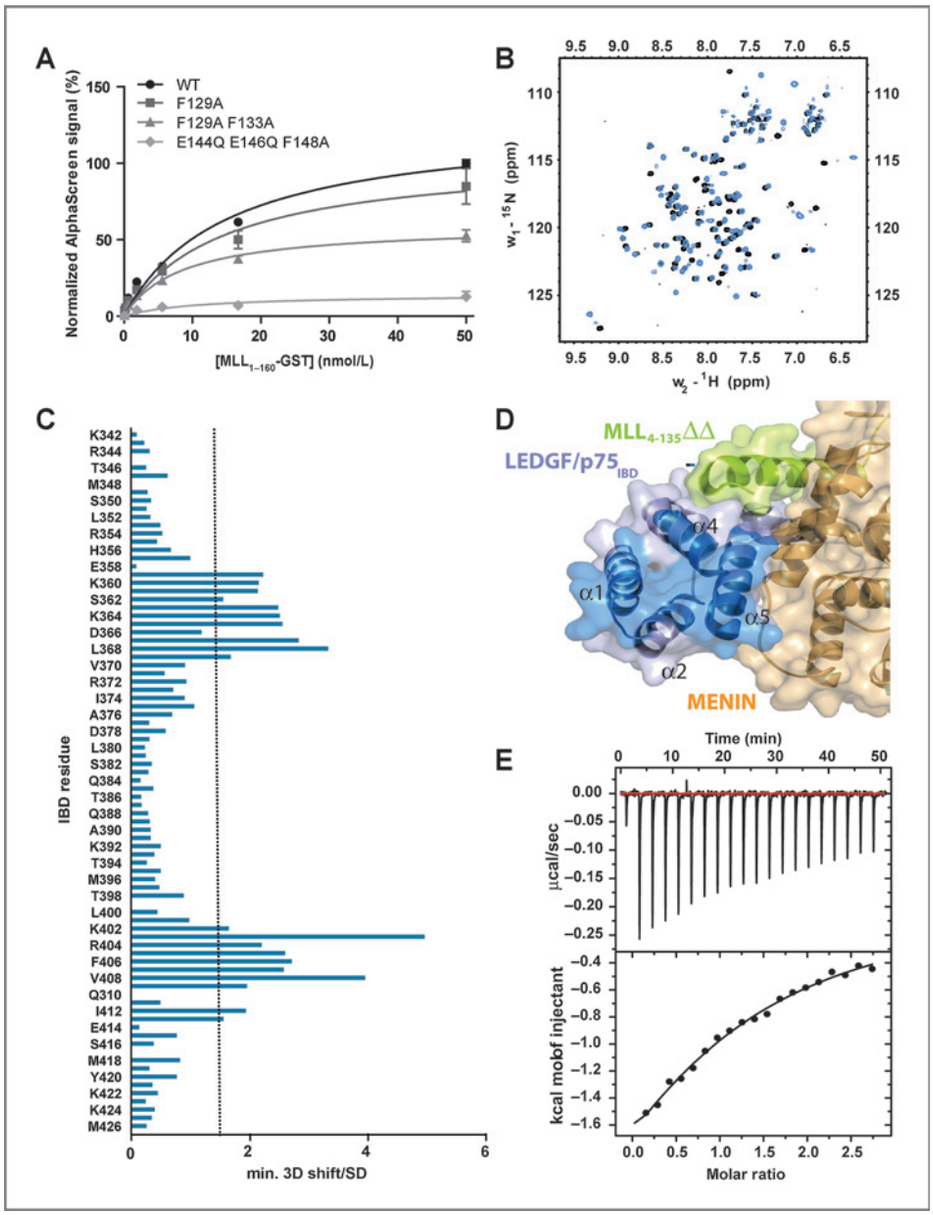

Figure 2. Identification of the LEDGF/p75–MLL interaction surface. A, mutational analysis of the interaction between LEDGF/p75 and MLL. Different amounts of $MLL_{1–160}$–GST (WT) or its indicated mutants were titrated against Flag-LEDGF/p75 (0.3 nmol/L). Binding was monitored in an AlphaScreen assay. Error bars, SD calculated from three independent experiments performed in duplicate. B, comparison of the NMR 2D $^{15}N/^{1}H$ HSQC spectra of the IBD in the absence (black) and presence (blue) of $MLL_{140–160}$. The spectra were obtained from the ^{15}N-labeled recombinant IBD and an unlabeled synthetic MLL-derived peptide. C, representation of the minimal chemical shift in backbone amide signals of the IBD upon addition of $MLL_{140–160}$. The graph summarizes the minimal chemical shift values divided by corresponding SD for backbone resonances. Backbone amide signals (^{15}N and ^{1}H) were assigned for all residues of the IBD except E345, M348, Q410, and T417. D, diagram depicting significantly shifted amino acid residues at the surface of the IBD as determined by NMR spectroscopy. Significantly shifted IBD amino acid residues were highlighted (dark blue) in the ternary structure representing MENIN (orange), the LEDGF/p75 IBD (light blue), and $MLL_{4–135}\Delta\Delta$ (green; PDB ID 3U88). E, ITC measurement of the IBD–$MLL_{140–160}$ interaction. Top, the experimental data; bottom, the fit of the integrated heats (full circles) from each injection of $MLL_{140–160}$.

regions (aa I359 to D369 and K402 to M413). These regions form two interhelical loops connecting IBD α helices α1–α2 and α4–α5, respectively. Significantly shifted amino acid residues were highlighted (dark blue) in Fig. 2D (25, 38).

Binding of $MLL_{140–160}$ to the IBD was further investigated using ITC. The ITC results corresponded with a stoichiometry close to 1:1 ($n = 1.15$). They were fitted by a single-site binding model, which provided the dissociation constant (K_d) of 86.3 ± 21.3 μmol/L (Fig. 2E). These results confirmed the existence of an additional interface between LEDGF/p75 and MLL.

Structural analysis of the MLL–LEDGF/p75 IBD interface

To obtain detailed insight into the mechanism of MLL recognition by LEDGF/p75, we determined the solution structure of the LEDGF/p75 IBD in complex with $MLL_{140–160}$. Comprehensive backbone and side-chain resonance assignments for the $MLL_{140–160}$-bound $^{13}C/^{15}N$-labeled LEDGF/p75 IBD were obtained using established triple-resonance experiments (31, 32) and for the bound unlabeled $MLL_{140–160}$ peptide using $^{13}C/^{15}N$-filtered homonuclear TOCSY and NOESY experiments. The essentially complete ^{15}N, ^{13}C, and ^{1}H resonance assignments allowed automated assignment of the NOEs identified in 3D $^{15}N/^{1}H$ NOESY-HSQC, $^{13}C/^{1}H$ HSQC-NOESY, and in 2D $^{13}C/^{15}N$-filtered/edited NOESY spectra using the CANDID protocol implemented in Cyana (35). This yielded unique assignments for 95.7% (2,338/2,444) of the NOE peaks observed, providing 1,313 nonredundant ^{1}H-^{1}H distance constraints, including 1,199 intra-LEDGF/p75 IBD, 78 intra-$MLL_{140–160}$, and 36 intermolecular constraints. Fifty-nine

converged structures for the LEDGF/p75 IBD–$MLL_{140–160}$ complex with no distance violations >0.2 Å were obtained from 100 random starting conformations using 1,451 NMR-derived structural constraints (~14.8 constraints per residue). The 20 lowest energy conformers were further refined in explicit solvent in YASARA (39). Structural statistics for the final water-refined set of structures are shown in Supplementary Table S2. The structures, NMR constraints and resonance assignments have been deposited in the Protein Data Bank (PDB, accession number 2msr) and BMRB database (accession number 25130).

Detailed analysis of the NOESY data revealed that the interaction of $MLL_{140–160}$ with the LEDGF/p75 IBD is maintained exclusively by the aromatic side-chains of two phenylalanine residues (F148 and F151), as illustrated by a region of the 2D $^{13}C/^{15}N$-filtered/edited NOESY spectrum in Fig. 3A. This observation is supported by the chemical shift changes in $MLL_{140–160}$ H^{α} or H^{N} proton signals upon binding to LEDGF/p75 IBD, which were identified in the region including $MLL_{140–160}$ residues E146-S153. The limited distribution of intermolecular distance constraints is reflected in a differential conformational behavior observed for both binding partners in the resulting structure of the LEDGF/p75 IBD–$MLL_{140–160}$ complex. The LEDGF/p75 IBD adopts a well-defined conformation that is highly similar to that found in the complex with HIV-1 integrase with backbone a root mean square deviation of 0.92 Å while $MLL_{140–160}$ remains relatively unstructured. $MLL_{140–160}$ is anchored between the two interhelical loops of LEDGF/p75 IBD (aa I359 to D369 and K402 to M413) via F148 and F151 (Fig. 3B). In addition, the lack of a defined conformation in the backbone region of bound $MLL_{140–160}$ between anchored residues F148 and F151 is in agreement with the absence of amide proton signals for G150 and F151 in NMR spectra due to exchange-related signal broadening. The aromatic ring of F148 resides in a relatively shallow hydrophobic pocket characterized by a number of NOE contacts with backbone and side-chain protons from L363, L368, I403, F406, K407, and V408 (Fig. 3C). In contrast, F151 is buried in a deeper pocket and its position is defined by an extensive network of NOEs including side-chain protons from I359, K360, L363, T399, K402, and I403. To corroborate the NMR structure, F148A and F151A single mutations and the F148A, F151A double-mutant were introduced in $MLL_{1–160}$–GST. The integrity of purified proteins was verified by SDS-PAGE (Supplementary Fig. S3) and their binding ability to Flag-LEDGF/p75 was tested in an *in vitro* AlphaScreen assay (Fig. 3D). As expected, both F148A and F151A mutations affected interaction of $MLL_{1–160}$–GST and Flag-LEDGF/p75, however, residual binding subsisted. The F148A-F151A double mutation reduced the binding comparably.

To develop a full model of the ternary complex, a representative NMR structure of $MLL_{140–160}$ bound to the IBD was superimposed on the previously published crystal structure of the ternary complex (PDB ID 3U88) in Chemical Computing Group's Molecular Operating Environment 2012.10 (25, 40). Loop modeling resulted in a model of the IBD–MENIN complex binding one chimeric MLL polypeptide chain combining available structural information Fig. 3E. This model also gives a possible explanation for the fact that the triple E144Q-E146Q-F148A mutant is more effective in abolishing of the interaction with LEDGF/p75 than the F148A-F151A double mutant (Fig. 3D). Introduction of opposite charge into the modeled loop of MLL most likely complemented the inhibitory effect of the F148A mutation.

The MLL and HIV-1 binding domains in LEDGF/p75 overlap but are not identical

The structure of the LEDGF/p75 IBD in complex with the HIV-1 integrase core domain has been resolved by X-ray crystallography (26, 38). The NMR-derived structure of the IBD–$MLL_{140–160}$ complex clearly shows an overlap between the MLL and HIV-1 integrase interfaces on the IBD (Fig. 4A). HIV-1 integrase W131, one of the vital residues for interaction with the IBD (26), and MLL F148 share a hydrophobic pocket on the IBD surface. The binding site of MLL F151, however, is not occupied by any of the HIV-1 integrase side-chains. Both proteins interact with IBD residues K360, L363, I365, L368, K402, I403, F406, and V408. In addition to these residues, only I359 and T399 are unique for the interaction with $MLL_{140–160}$, while IBD residues K364, D366, N367, and V370 participate in binding to HIV-1 integrase but not to MLL. Interestingly, LEDGF/p75 D366, a key residue for the HIV-1 integrase interaction (38), is largely buried upon interaction of the IBD with integrase but remains fully exposed upon MLL binding (Supplementary Table S3). Indeed, $MLL_{1–160}$–GST binding to Flag-LEDGF/p75 was not affected by the presence of a D366N substitution as measured by AlphaScreen (Fig. 4B). To evaluate mutually exclusive binding of MLL and HIV-1 integrase to LEDGF/p75, a competition experiment was performed. As expected, recombinant C-terminally His-tagged HIV-1 integrase could outcompete the interaction of Flag-LEDGF/p75 with $MLL_{1–160}$–GST in an AlphaScreen assay with a apparent IC_{50} of 39.7 nmol/L [95% confidence interval (CI), 32.6–50.0; Fig. 4C]. In the presence of LEDGF/p75 D366N, the IC_{50} increased 10-fold (IC_{50}, 447.9 nmol/L; 95% CI, 309.2–648.7), corroborating the specificity of the competition (Fig. 4C).

In addition, our latest NMR data defining the interaction of the LEDGF/p75 IBD with the cellular interaction partners JPO2 and PogZ revealed that these proteins also share the same interface on the IBD (unpublished data). We therefore purified full-length JPO2 and the transposase-derived C-terminus comprising the DDE domain of PogZ (aa 1117–1410), known to bind the LEDGF/p75 IBD (17, 18, 26) as N-terminal MBP fusions (MBP-JPO2 and MBP-PogZ, respectively). Unlike MBP alone, both proteins efficiently outcompeted MLL from the LEDGF/p75–MLL complex with apparent IC_{50} values of 26.6 nmol/L (95% CI, 21.1–33.4) and 8.7 nmol/L (95% CI, 6.6–11.6), respectively (Fig. 4D).

Selection of LEDGF/p75 mutants defective for interaction with MLL

On the basis of the structure of the LEDGF/p75–MLL complex, we predicted several mutations in LEDGF/p75 that would interfere with the interaction and assessed their ability to bind $MLL_{111–160}$–GST. Exposed amino acid residues located in the newly defined MLL binding site were targeted. An overview of all analyzed mutants and their effect on the MLL

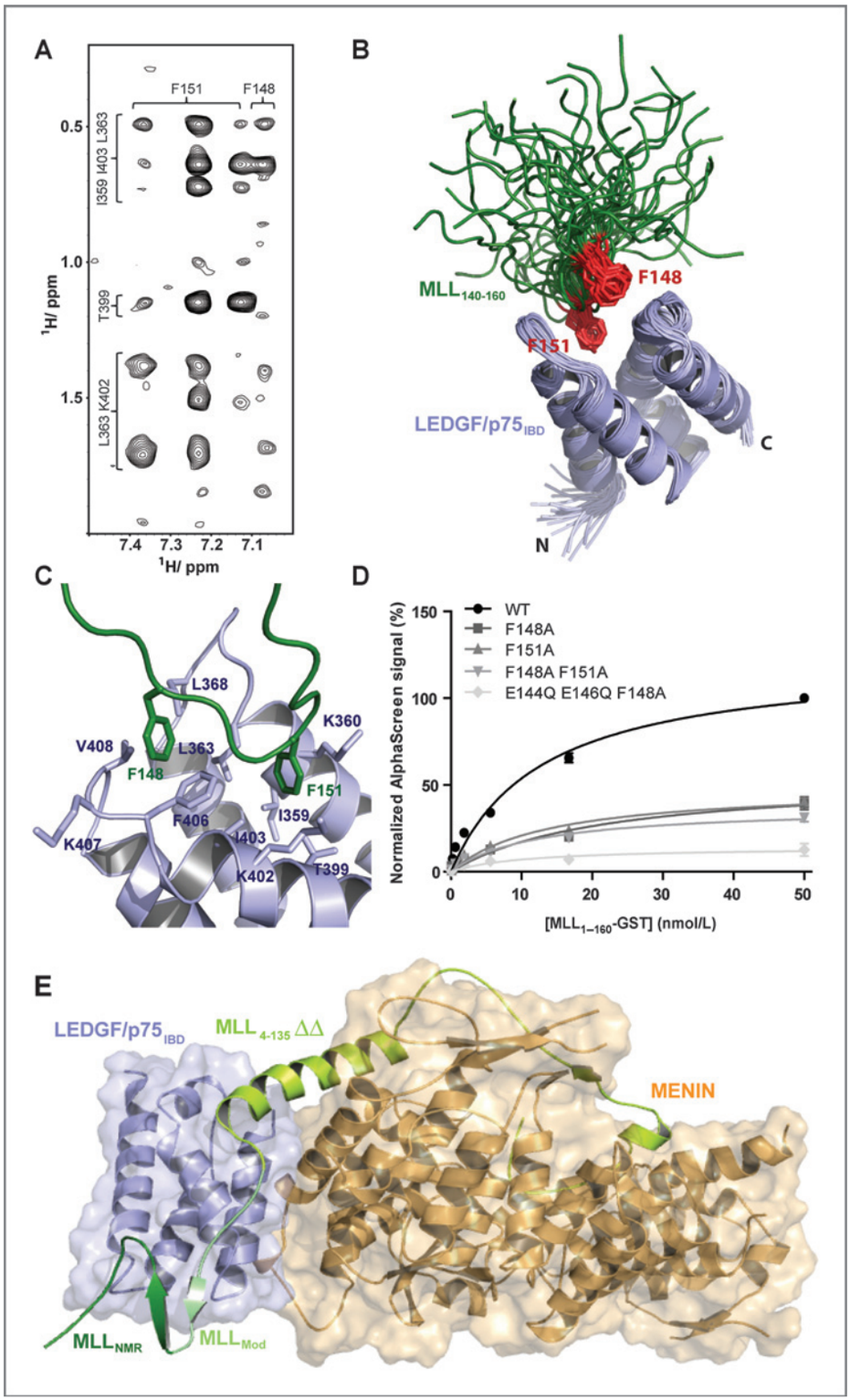

Figure 3. Model of the ternary MLL–MENIN-IBD structure. A, region from the 2D $^{13}C/^{15}N$-filtered/edited NOESY spectrum obtained for the LEDGF/p75 IBD–MLL$_{140–160}$ complex. The spectrum shows intermolecular NOE contacts between protons from $^{13}C/^{15}N$-labeled LEDGF/p75 IBD (*y*-axis) and unlabeled MLL$_{140–160}$ complex (*x*-axis). The spectral analysis reveals that the interaction between the molecules is exclusively maintained by the two aromatic side-chains of MLL F148 and F151. B, converged structures determined by NMR (PDB ID 2msr). The IBD is depicted in blue, MLL in green. MLL F148 and F151 are highlighted in red. The structures are overlaid on the LEDGF/p75 IBD secondary structure elements. C, detailed view of the MLL$_{140–160}$–LEDGF/p75 IBD interface. The diagrams show a representative NMR structure of MLL$_{140–160}$ (green) in complex with the LEDGF/p75 IBD (blue). MLL F148 binds into a hydrophobic pocket on the IBD surface formed by L363, L368, I403, F406, K407, and V408 and MLL F151 is buried in a pocket formed by I359, K360, L363, T399, K402, and I403. D, the F148A and F151 mutations affect LEDGF/p75–MLL interaction. Recombinant WT, F148A, or F151A single mutants or a F148A-F151A double mutant of MLL were titrated against 0.3 nmol/L LEDGF/p75 in an AlphaScreen experiment. The E144Q-E146Q-F148A mutant was analyzed in parallel to enable the comparison with Fig. 2A. Error bars, SDs calculated from three independent experiments performed in duplicate. E, model of the MLL–MENIN–LEDGF/p75 ternary complex. The published crystal structure of the ternary complex (PDB ID 3U88) and a representative NMR structure were used as a template. MENIN is depicted in orange and the LEDGF/p75 IBD in blue. The MLL$_{4–135}\Delta\Delta$ peptide derived from the crystal structure is depicted in lime green. The part of MLL derived from the NMR measurements (MLL$_{NMR}$) is shown in dark green and the modeled loop (MLL$_{Mod}$) in pale green. A detail of the interface is presented in Supplementary Fig. S6.

interaction is presented in Supplementary Tables S4 and S5. The integrity of purified WT Flag-LEDGF/p75 and interaction-defective mutants was verified by SDS-PAGE (Supplementary Fig. S3). Folding of these interaction-defective mutants was additionally analyzed by differential scanning fluorimetry (DSF; Supplementary Fig. S5 and Supplementary Table S6). The melting curves of all Flag-LEDGF/p75 mutants used in this study were comparable with that of WT Flag-LEDGF/p75.

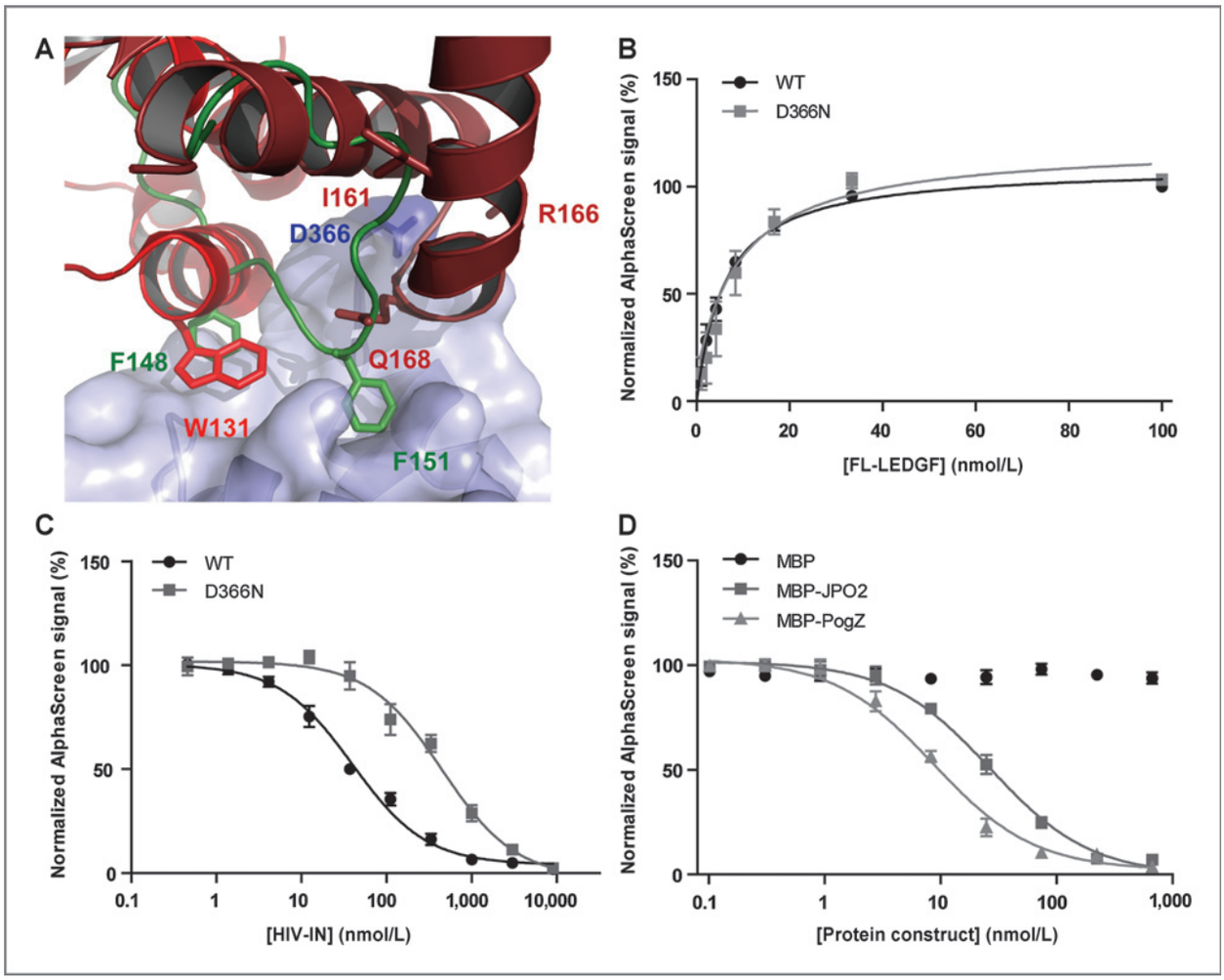

Figure 4. MLL, Jpo2, PogZ, and HIV-1 integrase share the same binding interface on the IBD. A, comparison of the HIV-1 integrase-, and MLL–LEDGF/p75 interaction. HIV-1 integrase W131, I161, R166, and Q168 (red) are known to be important for the HIV-1 integrase–LEDGF/p75 interaction. HIV-1 integrase W131 and MLL F148 (dark green) occupy the same hydrophobic pocket on the IBD (light blue) surface. MLL F151 does not compete with any of HIV-1 integrase side chains. D366 (dark blue) of the IBD is crucial for interaction with HIV-1 integrase, but not for interaction with $MLL_{140–160}$. The structure of the IBD–HIV-1 integrase interface was previously described (PDB ID 2B4J). B, the LEDGF/p75 D366N mutation, defective for HIV-1 integrase binding, does not affect binding of $MLL_{1–160}$–GST. Recombinant WT or D366N mutant Flag-LEDGF/p75 was titrated against 1 nmol/L $MLL_{1–160}$–GST in an AlphaScreen assay. C, HIV-1 integrase impairs the LEDGF/p75–MLL interaction *in vitro.* The interaction between recombinant WT or D366N mutant Flag-LEDGF/p75 (0.3 nmol/L) and $MLL_{1–160}$–GST (1 nmol/L) was monitored in an AlphaScreen assay, while an increasing amount of HIV-1 integrase (HIV-IN) was added. D, Jpo2 and PogZ inhibit the LEDGF/p75–MLL interaction *in vitro*. Recombinant MBP, MBP-JPO2, or MBP-PogZ (aa 1117–1410) were titrated against a fixed concentration of Flag-LEDGF (0.3 nmol/L) and $MLL_{1–160}$–GST (1 nmol/L) in an AlphaScreen assay. Error bars, SDs calculated from three independent experiments performed in duplicate.

A moderate reduction in the AlphaScreen signal was observed with the LEDGF/p75 L368A mutant (Fig. 5A) that contributes to formation of the hydrophobic pocket important for interaction with MLL residue F148 (Fig. 3C). This effect was increased when K407D was additionally mutated (L368A-K407D). A comparable effect was obtained with the R404D-R405D double mutant (Fig. 5B). R404, R405, and K407 most likely interact with negatively charged side-chains in the flexible loop connecting the fragment of MLL from the resolved crystal and the NMR structure (Supplementary Fig. S6; ref. 25). Residual binding may subsist in both cases due to the interaction supported by MLL F151, F129, and F133. We also tested a subset of point mutants known to be defective for interaction with HIV-1 integrase (38). None of these mutations significantly affected the binding to MLL, supporting the notion that their binding domains overlap but involve different residues of the IBD (Supplementary Table S5 and Supplementary Fig. S7).

The LEDGF/p75–MLL interface is important for LEDGF/p75-dependent MLL fusion–mediated leukemias

Knockdown of LEDGF/p75 expression impaires the clonogenic growth of MLL fusion–transformed hematopoietic cells (12, 23). To evaluate the importance of the newly defined LEDGF/p75–MLL interface, we analyzed whether the reduced colony-forming capacity of $MLL–AF9^{+}$ leukemic cells upon LEDGF/p75 knockdown could be rescued by overexpression of

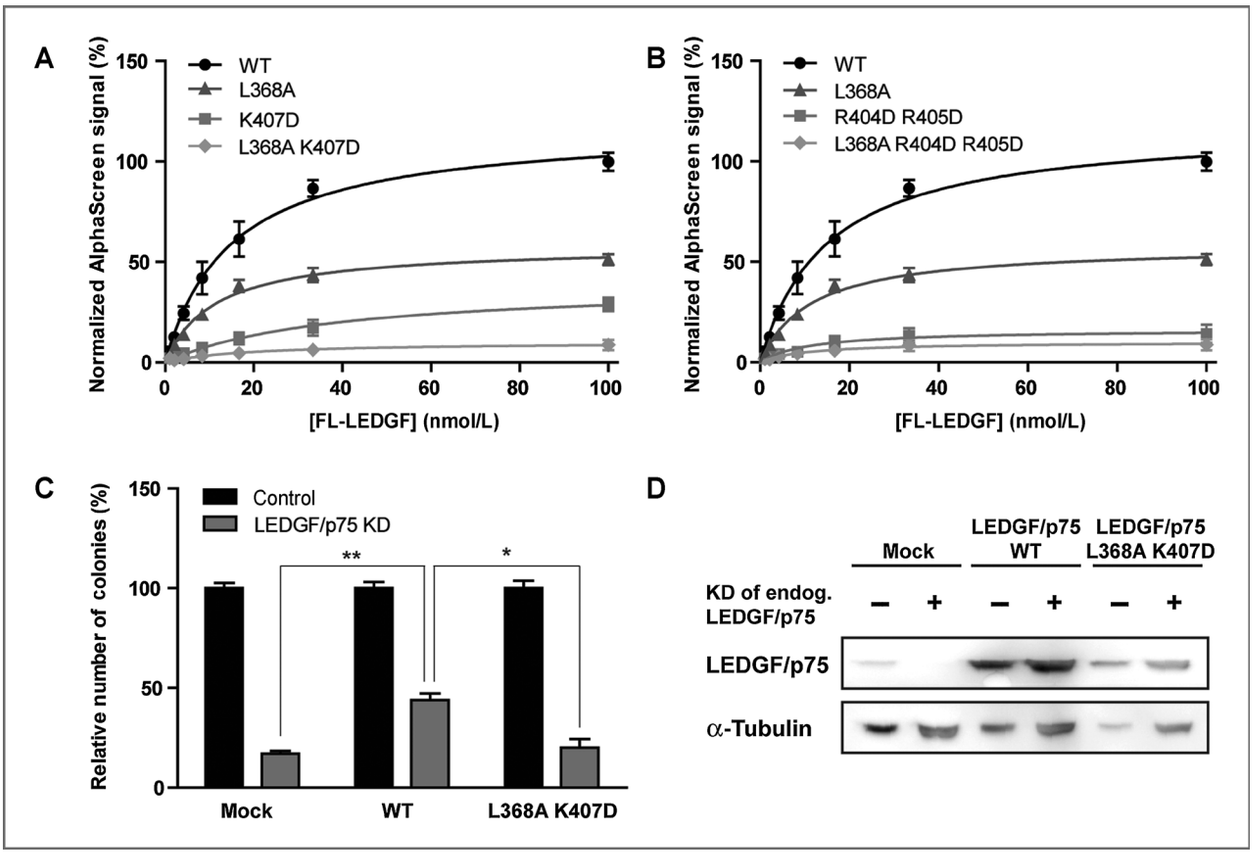

Figure 5. A MLL interaction-deficient LEDGF/p75 mutant cannot rescue MLL–AF9 transformation upon knockdown of endogenous LEDGF/p75. A and B, affinity of the indicated Flag-LEDGF/p75 mutants for $MLL_{111–160}$–GST. Recombinant WT or mutated Flag-LEDGF/p75 was titrated against 10 nmol/L of $MLL_{111–160}$–GST in an AlphaScreen Assay. Error bars, SDs calculated from three independent experiments performed in duplicate. C, THP1 cells were transduced with an empty vector (Mock) or a vector encoding WT miRNA-resistant LEDGF/p75 or the interaction-deficient mutant L368A-K407D. After selection of transduced cells, cells were transduced with an eGFP vector (control) or a vector expressing eGFP and a LEDGF/p75 miRNA (LEDGF/p75 knockdown). The colony-forming capacity was compared with the control cells (set at 100%). Error bars, SDs of a triplicate experiment; *, $P < 0.05$; **, $P < 0.005$, Student *t* test. D, levels of LEDGF/p75 and α-tubulin in the cells described in C were determined by Western blot analysis.

WT and/or the L368A-K407D LEDGF/p75 mutant. First, MLL–$AF9^+$ THP1 cells stably transduced with an empty vector (Mock) or a vector expressing WT or L368A-K407D–mutant LEDGF/p75 were generated. These cell lines were subsequently transduced with a lentiviral vector expressing eGFP (control) or eGFP together with a LEDGF/p75-specific miRNA to knockdown expression of endogenous LEDGF/p75 (LEDGF/p75 knockdown). The transduction efficiency was analyzed by FACS (>80%) and cells were subsequently seeded in methylcellulose. In the absence of LEDGF/75 backcomplementation (Mock), an 80% decrease in colonies could be observed upon LEDGF/p75 knockdown compared with the GFP control ($P < 0.0001$; Fig. 5C). In contrast, after backcomplementation with WT LEDGF/p75, the relative amount of colonies increased to 43% ($P = 0.0016$), whereas no rescue was be observed for LEDGF/p75 L368A-K407D. The knockdown of LEDGF/p75 was verified by Western blot analysis (Fig. 5D). Moreover, in absence of LEDGF/p75 (Mock) or upon LEDGF/p75 L368A-K407D overexpression, the remaining colonies in LEDGF/p75 knockdown conditions were phenotypically smaller compared with the GFP control (Supplementary Fig. S8). These results indicate that the identified LEDGF/p75–MLL interface is important for the maintenance of transformation by the MLL–AF9 fusion.

Expression of IBD-interacting peptides selectively impairs clonogenic growth of murine MLL fusion–expressing leukemic cells

The results discussed above show that besides the binding pocket formed by the MLL–MENIN interaction, LEDGF/p75 also interacts with MLL via a second interface that overlaps with the JPO2, PogZ, and HIV-1 integrase binding site. Using phage display, we previously identified cyclic peptides that inhibit the LEDGF/p75–HIV-1 integrase interaction and block viral replication at the integration step (27). Saturation transfer difference NMR spectroscopy (STD-NMR) indicated that these peptides bind specifically to the LEDGF/p75 IBD. We therefore evaluated the effect of one of these peptides (CP65) on MLL transformation. First, the impact of CP65 on the LEDGF/p75–MLL and MLL–MENIN interaction was investigated *in vitro* with recombinant proteins; MBP-tagged WT peptide (CP65-MBP, CILGHSDWCGGGK-MBP), a partial interaction-

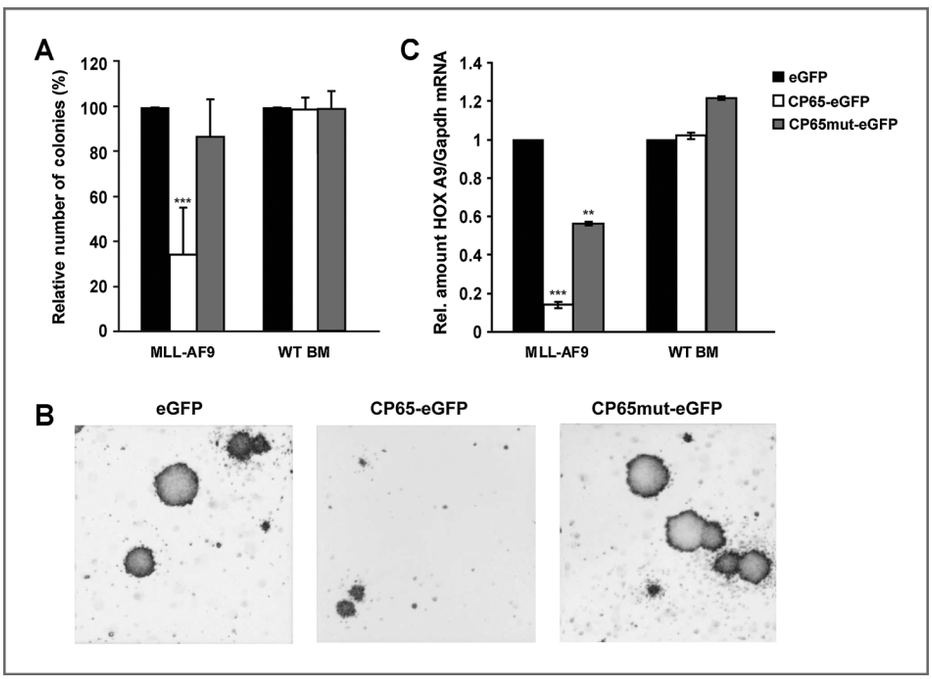

Figure 6. LEDGF/p75 IBD interacting cyclic peptides impair colony formation of MLL–AF9-expressing murine leukemic blasts. A, MLL–AF9-transformed leukemic blasts derived from murine AML or WT bone marrow progenitors (WT BM) cells were transduced with a MSCV-derived vector expressing eGFP or eGFP fused to the cyclic peptide CP65 (CP65-eGFP) or a partialy interaction defective mutant (CP65mut-eGFP). The colony-forming capacity was compared with the eGFP control (set at 100%). B, representative colonies for each condition. C, *HOXA9* expression of the cells depicted in A was determined by qRT-PCR. Expression levels were normalized to the eGFP control using *Gapdh* as a reference gene. Error bars, SD of three independent experiments. **, $P < 0.01$; ***, $P < 0.001$, ANOVA with Tukey multiple comparison test.

defective mutant (CP65mut-MBP, CILGHSDACGGGK-MBP), and a scrambled peptide (CP65scr-MBP, GCGLSCGWKGIHD-MBP) were produced and validated in an AlphaScreen assay. As shown in Supplementary Fig. S9A, WT CP65-MBP displaced Flag-LEDGF/p75 from MLL_{1-160}–GST with approximately 6-fold lower apparent IC_{50} than CP65mut-MBP, while the CP65scr-MBP did not affect LEDGF/p75–MLL complex formation. As expected, none of these tagged peptides interfered with the interaction of MLL_{1-160}–GST and His–TRX–tagged MENIN (Supplementary Fig. S9B).

Next, the effect of CP65 on MLL fusion–mediated cellular transformation was investigated. To this purpose, we expressed CP65 in primary murine MLL–AF9-expressing leukemic blasts isolated from mice developing AML after transplantation with MLL–AF9-expressing bone marrow progenitors. As shown previously, the disease is characterized by multiorgan invasion of leukemic cells, such as in the spleen, leading to splenomegaly (23, 30). These cells were characterized by expression of the early progenitor cell surface markers such as c-kit and FcγRI/II as well as the myeloid markers Gr-1 and Mac-1 and by increased expression of known MLL target genes such as the Hoxa cluster *Hoxa9*, *Hoxa7*, and *Meis1* (Supplementary Fig. S2; ref. 41). Normal mouse bone marrow progenitors (WT BM) and the interaction-defective mutant peptide were used as controls (27). Cells were transduced with a MSCV-based retroviral vector (*pMSCV*) expressing the peptides as N-terminal eGFP fusions. Forty-eight hours after transduction, $eGFP^+$ cells were flow-sorted and seeded in methylcellulose containing hematopoietic growth factors (Supplementary Fig. S2). As shown in Fig. 6A, expression of CP65 reduced the number of MLL–AF9-expressing colonies by 66% ($P < 0.001$) and remaining colonies were smaller compared with the eGFP control (Fig. 6B), while expression of CP65mut did not significantly impair colony-forming capacity. In addition, lineage marker-depleted normal (WT) bone marrow was not affected by expression of the CP65 peptides (Fig. 6A). qRT-PCR analysis performed on cells harvested from methylcellulose indicated that expression of CP65 was associated with a significant reduction (86%; $P < 0.01$) of *HOXA9* mRNA levels. Expression of the mutant peptide also reduced *HOXA9* expression for 44% ($P < 0.01$) most likely due to residual binding of the peptide (Fig. 6C). These results suggest that the LEDGF/p75–MLL interaction interface is important for maintenance of LEDGF/p75-dependent MLL–AF9-mediated transformation and can be disrupted by a small peptide that binds to the LEDGF/p75 IBD.

Discussion

MLL fusion–driven acute leukemias represent a genetically distinct subset of leukemias often facing poor prognosis. Current research is focused on the development of more selective small-molecule inhibitors. Unlike WT MLL, the most prevalent MLL fusion partners directly or indirectly interact with the histone methyltransferase DOT1L (42, 43). DOT1L-mediated hypermethylation of H3K79 leads to aberrant expression of MLL target genes, such as *HOXA9* and *MEIS1* (44, 45). Therefore, DOTL1 is considered a promising drug target with several small-molecule inhibitors in development (45). Recently, the LEDGF/p75–MLL–MENIN complex was put forward as a new target alongside DOT1L (10–12, 23). Because nearly all N-terminal MLL fusions are expected to form this ternary complex, a potent inhibitor could target a substantial subset of MLL fusion–mediated leukemias. The interaction between MLL and MENIN is well described and promising small molecules targeting this interface have been identified (24). These

compounds bind to the central hydrophobic pocket of MENIN and thereby destabilize the LEDGF/p75–MLL–MENIN ternary complex. However, it has not been shown whether these compounds can be used without inducing cytotoxic effects. In this regard, MENIN functions as a tumor suppressor in endocrine tissues. Mutations in MENIN can induce multiple endocrine neoplasia type I (MEN1) and some clinical mutations have been shown to abrogate the interaction with LEDGF/p75 (12). The tumor suppression function of MENIN is related to its interaction with JUND (46). Structural data have indicated that the interaction of JUND with MENIN is highly similar to the MENIN–MLL interaction (25).

Recently, we showed that MLL fusion–mediated transformation can be inhibited by outcompeting LEDGF/p75 from the complex without blocking the MLL–MENIN interaction (23). This study also demonstrated that the LEDGF/p75–MLL interface represents a potential target to treat MLL-associated leukemias. Although only MLL–AF9 and MLL–ENL leukemias have been tested for their LEDGF/p75 dependency, we expect that like for MENIN inhibitors, all oncogenic MLL fusions retaining the MLL N-terminus are potential targets (12, 23). In addition, it was recently shown that MLL fusion leukemia also requires the presence of the WT MLL protein offering an additional target for LEDGF/p75–MLL inhibitors (8).

In this report, we show that MLL interacts with LEDGF/p75 via two distinct interfaces. The first interface is formed by the LEDGF/p75–MENIN complex as revealed in the previously published crystal structure (25). The interface described in this article overlaps with those established for interaction of HIV-1 integrase, JPO2, and PogZ interaction with the LEDGF/p75 IBD (unpublished data; refs. 16, 17). Structural NMR studies, including detailed characterization of the interaction between LEDGF/p75 and MLL-derived peptides, revealed that the second interface is maintained by two aromatic side-chains of MLL (Fig. 3). MLL F148 occupies a hydrophobic pocket on the IBD surface formed by L363, L368, I403, F406, K407, and V408 while MLL F151 is buried in a pocket formed by I359, K360, L363, T399, K402, and I403. Although the LEDGF/p75 IBD–MLL interface overlaps with that of HIV-1 integrase, the engaged IBD residues are not identical (Supplementary Fig. S7 and Supplementary Table S5).

The LEDGF/p75–HIV-1 integrase interaction is considered a novel target to treat HIV-1 infection. Small molecules disrupting this interaction (LEDGINs) bind HIV-1 integrase and avoid cellular toxicity (47). Recently, we reported that cyclic peptides and small molecules derived thereof that bind to the IBD, inhibit the interaction with HIV-1 integrase and viral replication (27, 48). Taking into account that the LEDGF/p75–MLL and LEDGF/p75–HIV-1 integrase interfaces overlap, we evaluated one of these peptides (CP65) as a potential inhibitor of the LEDGF/p75–MLL interaction. This peptide specifically blocked the LEDGF/p75–MLL interaction and affected MLL fusion–dependent leukemic transformation, supporting the amenability of the LEDGF/p75–MLL interface for therapeutic targeting (Fig. 6). However, at this point, it is not possible to determine whether CP65-mediated inhibition is exerted on the MLL fusion, WT MLL, or both of them.

Although earlier cellular experiments suggested that the LEDGF/p75–MLL interaction is dependent on the presence of MENIN (12, 23), our *in vitro* data suggest that LEDGF/p75 and MLL can interact in the absence of MENIN. Addition of MENIN in the LEDGF/p75–MLL *in vitro* interaction assay induces a 4-fold stimulation of the interaction (data not shown). It is still unclear how MENIN regulates the LEDGF/p75–MLL interaction and how the presence of MENIN influences MLL targeting. In this regard, a recent study by Artinger and colleagues (49) revealed that expression of some MLL-regulated genes is not dependent on MENIN, which might reflect the presence of a LEDGF/p75–MENIN independent chromatin tethering mechanism. The possibility that not all MLL target genes depend on the presence of LEDGF/p75 has important implications when considering the LEDGF/p75–MLL interaction as a new therapeutic target. Indeed, the function of the LEDGF/p75–MLL–MENIN complex has been studied in the context of MLL-mediated leukemic transformation but not in normal blood cell differentiation. The majority of LEDGF/p75 knockout mice die prenatally and display a phenotype reminiscent of a *Hoxa* gene knockout (22, 50). These results suggest that LEDGF/p75 is important for the function of MLL and to maintain *Hoxa* gene expression during embryogenesis. In light of future drug development, it will be of interest to evaluate the role of a LEDGF/p75 for normal hematopoiesis.

Despite a potential role in blood cell differentiation, LEDGF/p75-dependent MLL-regulated genes are critical to maintain leukemic transformation (12, 23). In addition to the MLL–MENIN interaction, our results suggest that the LEDGF/p75–MLL interaction should also be considered as a target to treat LEDGF/p75-dependent MLL leukemia. The finding that the LEDGF/p75–MLL interface overlaps with the LEDGF/p75–HIV integrase interface implies that we can exploit knowledge on the LEDGF/p75–HIV integrase interaction and drug development giving us a head start in the development of LEDGF/p75–MLL inhibitors.

Disclosure of Potential Conflicts of Interest

No potential conflicts of interest were disclosed.

Authors' Contributions

Conception and design: K. Čermáková, S. El Ashkar, J. Schwaller, V. Veverka, J. De Rijck

Development of methodology: K. Čermáková, S. El Ashkar, J. De Rijck

Acquisition of data (provided animals, acquired and managed patients, provided facilities, etc.): P. Tesina, H. Méreau, J. Schwaller, V. Veverka, J. De Rijck

Analysis and interpretation of data (e.g., statistical analysis, biostatistics, computational analysis): K. Čermáková, P. Tesina, J. Demeulemeester, H. Méreau, J. Schwaller, V. Veverka, J. De Rijck

Writing, review, and/or revision of the manuscript: K. Čermáková, P. Tesina, J. Demeulemeester, S. El Ashkar, H. Méreau, J. Schwaller, P. Řezáčová, V. Veverka, J. De Rijck

Administrative, technical, or material support (i.e., reporting or organizing data, constructing databases): K. Čermáková, P. Tesina, J. De Rijck

Study supervision: P. Řezáčová, J. De Rijck

Acknowledgments

The authors thank Milan Kozisek (IOCB AS CR) for his help with collection, processing, and analysis of ITC data, Martine Michiels (KU Leuven) for the excellent technical assistance, and the Leuven Viral Vector Core for the vector production.

Grant Support

This work was supported by the Research Foundation Flanders (FWO; G.0595.13 and KAN2012 1.5.108.12), the Flemish agency for Innovation by Science and Technology (IWT) SBO Interactomics (QPG-345523), the KU Leuven research fund (IDO/12/2008), the Ministry of Education of the Czech Republic [LK11205 (programme "NAVRAT"), 7E08066, and Project InterBioMed LO1302], projects (RVO 61388963) and (68378050) awarded by the Academy of Sciences of the Czech Republic and Grant Agency of the Charles University in Prague (1400–243–253355), the Swiss National Science Foundation (SNF-31003A-130661/1), the Swiss Cancer League (KFS-2778–02–2011), and the Gertrude von Meissner Foundation (Basel, Switzerland). K. Čermáková and J. Demeulemeester are supported by the FWO.

The costs of publication of this article were defrayed in part by the payment of page charges. This article must therefore be hereby marked *advertisement* in accordance with 18 U.S.C. Section 1734 solely to indicate this fact.

Received December 20, 2013; revised May 27, 2014; accepted June 10, 2014; published OnlineFirst July 23, 2014.

References

1. Krivtsov AV, Armstrong SA. MLL translocations, histone modifications and leukaemia stem-cell development. Nat Rev Cancer 2007;7:823–33.
2. Jude CD, Climer L, Xu D, Artinger E, Fisher JK, Ernst P. Unique and independent roles for MLL in adult hematopoietic stem cells and progenitors. Cell Stem Cell 2007;1:324–37.
3. McMahon KA, Hiew SY, Hadjur S, Veiga-Fernandes H, Menzel U, Price AJ, et al. Mll has a critical role in fetal and adult hematopoietic stem cell self-renewal. Cell Stem Cell 2007;1:338–45.
4. Meyer C, Hofmann J, Burmeister T, Groger D, Park TS, Emerenciano M, et al. The MLL recombinome of acute leukemias in 2013. Leukemia 2013;27:2165–76.
5. Lin C, Smith ER, Takahashi H, Lai KC, Martin-Brown S, Florens L, et al. AFF4, a component of the ELL/P-TEFb elongation complex and a shared subunit of MLL chimeras, can link transcription elongation to leukemia. Mol Cell 2010;37:429–37.
6. Bursen A, Schwabe K, Ruster B, Henschler R, Ruthardt M, Dingermann T, et al. The AF4.MLL fusion protein is capable of inducing ALL in mice without requirement of MLL.AF4. Blood 2010;115:3570–9.
7. Emerenciano M, Kowarz E, Karl K, de Almeida Lopes B, Scholz B, Bracharz S, et al. Functional analysis of the two reciprocal fusion genes MLL-NEBL and NEBL-MLL reveal their oncogenic potential. Cancer Lett 2013;332:30–4.
8. Thiel AT, Blessington P, Zou T, Feather D, Wu X, Yan J, et al. MLL–AF9–induced leukemogenesis requires coexpression of the wild-type Mll allele. Cancer Cell 2010;17:148–59.
9. Risner LE, Kuntimaddi A, Lokken AA, Achille NJ, Birch NW, Schoenfelt K, et al. Functional specificity of CpG DNA-binding CXXC domains in mixed lineage leukemia. J Biol Chem 2013;288:29901–10.
10. Grembecka J, Belcher AM, Hartley T, Cierpicki T. Molecular basis of the mixed lineage leukemia-menin interaction: implications for targeting mixed lineage leukemias. J Biol Chem 2010;285:40690–8.
11. Yokoyama A, Somervaille TC, Smith KS, Rozenblatt-Rosen O, Meyerson M, Cleary ML. The menin tumor suppressor protein is an essential oncogenic cofactor for MLL-associated leukemogenesis. Cell 2005;123:207–18.
12. Yokoyama A, Cleary ML. Menin critically links MLL proteins with LEDGF on cancer-associated target genes. Cancer Cell 2008;14:36–46.
13. De Rijck J, Bartholomeeusen K, Ceulemans H, Debyser Z, Gijsbers R. High-resolution profiling of the LEDGF/p75 chromatin interaction in the ENCODE region. Nucleic Acids Res 2010;38:6135–47.
14. Eidahl JO, Crowe BL, North JA, McKee CJ, Shkriabai N, Feng L, et al. Structural basis for high-affinity binding of LEDGF PWWP to mononucleosomes. Nucleic Acids Res 2013;41:3924–36.
15. Pradeepa MM, Sutherland HG, Ule J, Grimes GR, Bickmore WA. Psip1/Ledgf p52 binds methylated histone H3K36 and splicing factors and contributes to the regulation of alternative splicing. PLoS Genet 2012;8:e1002717.
16. Bartholomeeusen K, Christ F, Hendrix J, Rain JC, Emiliani S, Benarous R, et al.Lens epithelium-derived growth factor/p75 interacts with the transposase-derived DDE domain of PogZ. J Biol Chem 2009;284:11467–77.
17. Bartholomeeusen K, De Rijck J, Busschots K, Desender L, Gijsbers R, Emiliani S, et al. Differential interaction of HIV-1 integrase and JPO2 with the C terminus of LEDGF/p75. J Mol Biol 2007;372:407–21.
18. Cherepanov P, Maertens G, Proost P, Devreese B, Van Beeumen J, Engelborghs Y, et al. HIV-1 integrase forms stable tetramers and associates with LEDGF/p75 protein in human cells. J Biol Chem 2003;278:372–81.
19. Maertens G, Cherepanov P, Pluymers W, Busschots K, De Clercq E, D7ebyser Z, et al. LEDGF/p75 is essential for nuclear and chromosomal targeting of HIV-1 integrase in human cells. J Biol Chem 2003;278:33528–39.
20. Llano M, Saenz DT, Meehan A, Wongthida P, Peretz M, Walker WH, et al. An essential role for LEDGF/p75 in HIV integration. Science 2006;314:461–4.
21. Schrijvers R, De Rijck J, Demeulemeester J, Adachi N, Vets S, Ronen K, et al. LEDGF/p75-independent HIV-1 replication demonstrates a role for HRP-2 and remains sensitive to inhibition by LEDGINs. PLoS Pathog 2012;8:e1002558.
22. Shun MC, Raghavendra NK, Vandegraaff N, Daigle JE, Hughes S, Kellam P, et al. LEDGF/p75 functions downstream from preintegration complex formation to effect gene-specific HIV-1 integration. Genes Dev 2007;21:1767–78.
23. Mereau H, De Rijck J, Cermakova K, Kutz A, Juge S, Demeulemeester J, et al. Impairing MLL-fusion gene-mediated transformation by dissecting critical interactions with the lens epithelium-derived growth factor (LEDGF/p75). Leukemia 2013;27:1245–53.
24. Grembecka J, He S, Shi A, Purohit T, Muntean AG, Sorenson RJ, et al. Menin-MLL inhibitors reverse oncogenic activity of MLL fusion proteins in leukemia. Nat Chem Biol 2012;8:277–84.
25. Huang J, Gurung B, Wan B, Matkar S, Veniaminova NA, Wan K, et al. The same pocket in menin binds both MLL and JUND but has opposite effects on transcription. Nature 2012;482:542–6.
26. Cherepanov P, Ambrosio AL, Rahman S, Ellenberger T, Engelman A. Structural basis for the recognition between HIV-1 integrase and transcriptional coactivator p75. Proc Natl Acad Sci U S A 2005;102:17308–13.
27. Desimmie BA, Humbert M, Lescrinier E, Hendrix J, Vets S, Gijsbers R, et al. Phage display-directed discovery of LEDGF/p75 binding cyclic peptide inhibitors of HIV replication. Mol Ther 2012;20:2064–75.
28. Liu T, Jankovic D, Brault L, Ehret S, Baty F, Stavropoulou V, et al. Functional characterization of high levels of meningioma 1 as collaborating oncogene in acute leukemia. Leukemia 2010;24:601–12.
29. Ibrahimi A, Vande Velde G, Reumers V, Toelen J, Thiry I, Vandeputte C, et al. Highly efficient multicistronic lentiviral vectors with peptide 2A sequences. Hum Gene Ther 2009;20:845–60.
30. Schwaller J, Frantsve J, Aster J, Williams IR, Tomasson MH, Ross TS, et al. Transformation of hematopoietic cell lines to growth-factor independence and induction of a fatal myelo- and lymphoproliferative disease in mice by retrovirally transduced TEL/JAK2 fusion genes. EMBO J 1998;17:5321–33.
31. Renshaw PS, Veverka V, Kelly G, Frenkiel TA, Williamson RA, Gordon SV, et al. Sequence-specific assignment and secondary structure determination of the 195-residue complex formed by the Mycobacterium tuberculosis proteins CFP-10 and ESAT-6. J Biomol NMR 2004;30:225–6.
32. Veverka V, Lennie G, Crabbe T, Bird I, Taylor RJ, Carr MD. NMR assignment of the mTOR domain responsible for rapamycin binding. J Biomol NMR 2006;36:3.
33. Cheng X, Veverka V, Radhakrishnan A, Waters LC, Muskett FW, Morgan SH, et al. Structure and interactions of the human programmed cell death 1 receptor. J Biol Chem 2013;288:11771–85.
34. Wilkinson IC, Hall CJ, Veverka V, Shi JY, Muskett FW, Stephens PE, et al. High resolution NMR-based model for the structure of a scFv-

IL-1beta complex: potential for NMR as a key tool in therapeutic antibody design and development. J Biol Chem 2009;284: 31928–35.
35. Herrmann T, Guntert P, Wuthrich K. Protein NMR structure determination with automated NOE assignment using the new software CANDID and the torsion angle dynamics algorithm DYANA. J Mol Biol 2002;319:209–27.
36. Shen Y, Delaglio F, Cornilescu G, Bax A. TALOS^{+}: a hybrid method for predicting protein backbone torsion angles from NMR chemical shifts. J Biomol NMR 2009;44:213–23.
37. Doreleijers JF, Sousa da Silva AW, Krieger E, Nabuurs SB, Spronk CA, Stevens TJ, et al. CING: an integrated residue-based structure validation program suite. J Biomol NMR 2012;54:267–83.
38. Cherepanov P, Sun ZY, Rahman S, Maertens G, Wagner G, Engelman A. Solution structure of the HIV-1 integrase-binding domain in LEDGF/p75. Nat Struct Mol Biol 2005;12:526–32.
39. Harjes E, Harjes S, Wohlgemuth S, Muller KH, Krieger E, Herrmann C, et al. GTP-Ras disrupts the intramolecular complex of C1 and RA domains of Nore1. Structure 2006;14:881–8.
40. MOE. Molecular Operating Environment. Montreal, QC, Canada: Chemical Computing Group Inc.; 2012.
41. Faber J, Krivtsov AV, Stubbs MC, Wright R, Davis TN, van den Heuvel-Eibrink M, et al. HOXA9 is required for survival in human MLL-rearranged acute leukemias. Blood 2009;113:2375–85.
42. Mohan M, Lin C, Guest E, Shilatifard A. Licensed to elongate: a molecular mechanism for MLL-based leukaemogenesis. Nat Rev Cancer 2010;10:721–8.
43. Okada Y, Feng Q, Lin Y, Jiang Q, Li Y, Coffield VM, et al. hDOT1L links histone methylation to leukemogenesis. Cell 2005;121:167–78.
44. Bernt KM, Zhu N, Sinha AU, Vempati S, Faber J, Krivtsov AV, et al. MLL-rearranged leukemia is dependent on aberrant H3K79 methylation by DOT1L. Cancer Cell 2011;20:66–78.
45. Daigle SR, Olhava EJ, Therkelsen CA, Majer CR, Sneeringer CJ, Song J, et al. Selective killing of mixed lineage leukemia cells by a potent small-molecule DOT1L inhibitor. Cancer Cell 2011;20: 53–65.
46. Agarwal SK, Guru SC, Heppner C, Erdos MR, Collins RM, Park SY, et al. Menin interacts with the AP1 transcription factor JunD and represses JunD-activated transcription. Cell 1999;96:143–52.
47. Christ F, Voet A, Marchand A, Nicolet S, Desimmie BA, Marchand D, et al. Rational design of small-molecule inhibitors of the LEDGF/p75-integrase interaction and HIV replication. Nat Chem Biol 2010; 6:442–8.
48. Cavalluzzo C, Christ F, Voet A, Sharma A, Singh BK, Zhang KY, et al. Identification of small peptides inhibiting the integrase-LEDGF/p75 interaction through targeting the cellular co-factor. J Pept Sci 2013;19: 651–8.
49. Artinger EL, Mishra BP, Zaffuto KM, Li BE, Chung EK, Moore AW, et al. An MLL-dependent network sustains hematopoiesis. Proc Natl Acad Sci U S A 2013;110:12000–5.
50. Sutherland HG, Newton K, Brownstein DG, Holmes MC, Kress C, Semple CA, et al. Disruption of Ledgf/Psip1 results in perinatal mortality and homeotic skeletal transformations. Mol Cell Biol 2006;26: 7201–10.